Green Chemistry

Accepted Manuscript

This article can be cited before page numbers have been issued, to do this please use: X. Pei, D. xiong, Y. Pei, H. Wang and J. Wang, *Green Chem.*, 2018, DOI: 10.1039/C8GC00801A.

ROYAL SOCIETY OF CHEMISTRY

rsc.li/green-chem

View Article Online
DOI: 10.1039/C8GC00801A

Journal Name

ARTICLE

Switchable oil-water phase separation of ionic liquids based microemulsions by CO_2

Received 00th January 20xx,
Accepted 00th January 20xx

DOI: 10.1039/x0xx00000x

www.rsc.org/

Xiaoyan Pei, Dazhen Xiong, Yuanchao Pei, Huiyong Wang and Jianji Wang*

Phase separation of microemulsions plays an important role in many applications such as oil recovery, nanomaterials synthesis, and chemical reactions. However, reversible switching from ionic liquids based microemulsions to complete oil - water phase separation has not been reported so far. In this work, we developed a novel class of stimuli-responsive microemulsions composed of CO_2-responsive ionic liquid, n-pentanol and water. The microstructures and phase behavior of the microemulsion systems before and after bubbling of CO_2 were investigated by electrical conductivity, dynamic light scattering, small-angle X-ray scattering, cryogenic transmission electron microscopy, and optical microscope. It was found that these microemulsions could be reversibly switched from W/O monophase to complete oil - water phase separation upon alternatively bubbling and removal of CO_2 at atmospheric pressure. Furthermore, ^{13}C NMR spectroscopy was used to understand the CO_2-driven reversible phase separation of the microemulsions. The results suggest that the mechanism behind the reversible phase separation involved the reversible formation of bicarbonate and carbamate from the reaction between CO_2 and anions of the ionic liquids in the presence of water, which resulted in the increase of ionic strength (or vice versa) in the mixture. By using the microemulsions as microreactors, the phase separation protocol was applied in Knoevenagel reaction for efficient coupling of chemical reaction, product separation, and recycling of the microemulsions.

Introduction

Microemulsions are thermodynamically stable, optically clear and isotropic mixtures of oil, water and surfactant.[1] They have a broad range of applications in pharmaceuticals,[2] organic catalysis,[3] oil recovery,[4] drug delivery,[5] and nanoparticle synthesis.[6] In these applications, microemulsions often need to be temporarily stabilized for the reactions and subsequently demulsified for products separation. Thus de-emulsification of microemulsions is also critical in practical applications. Traditional destabilization methods of microemulsions include pervaporation,[7] temperature-induced instability, and addition of electrolytes or solvents,[8,9] which are usually less sustainable due to the high energy input and irreversible change in system composition. Therefore, it is of significance to develop efficient strategies for reversible formation and disruption of microemulsions for green and sustainable processes.

One of the important strategies is to develop stimuli-responsive microemulsions. For this purpose, a number of surfactants together with additives have been used to formulate stimuli-responsive microemulsions which can be reversibly destabilized and regenerated with different triggers. For example, Tabor et al.[10] reported a light-responsive reversible phase separation of water-in-decane microemulsion stabilized by sodium bis(2-ethyl-hexyl)sulfosuccinate (AOT) through doping sodium 4-butylphenyldiazenylphenoxybutane-1-sulfonate (AZOT-S4) into the system. Upon exposure to UV light of different wavelengths, the AZOT-S4 exhibited reversible trans–cis isomerization, resulting in reversible phase separation of the microemulsion. Zhang et al.[11] found a CO_2-switchable n-heptane-in-water microemulsion stabilized with sodium dodecyl sulphate (SDS) by introducing N,N-dimethyl-N-dodecyl amine ($C_{12}A$) into the O/W system. Upon alternatively bubbling and removal of CO_2, disruption and re-formation of the microemulsion could be achieved based on the response of $C_{12}A$ to CO_2. Recently, Liu et al.[12] demonstrated a CO_2-switchable bicontinuous microemulsion by using N,N,N',N'-tetramethyl-1,3-propanediamine (TMPDA), SDS, n-hexane, n-butanol and water, and the reversible switching from monophasic bicontinuous microemulsion to complete phase separation could be achieved for several cycles owing to the CO_2-responsive performance of TMPDA. However, in these switchable microemulsions, stimuli-responsive additives have to be used, which complicated the microemulsions composition and the components recovery.

Another viable option is ionic liquids (ILs) based stimuli-responsive microemulsions, where ILs are nonvolatile and their structures and properties are tunable for a specific purpose.[13-15] In this context, Brown et al.[16] reported a CO_2-responsive nonaqueous microemulsion containing cyclohexane and two different ionic liquids: 1-hexadecyl-3-methylimidazolium

Collaborative Innovation Center of Henan Province for Green Manufacturing of Fine Chemicals, Henan Key Laboratory of Green Chemistry, Key Laboratory of Green Chemical Media and Reactions, Ministry of Education, School of Chemistry and Chemical Engineering, Henan Normal University, Xinxiang, Henan 453007, P. R. China. E-mail: Jwang@htu.cn

Electronic Supplementary Information (ESI) available. See DOI: 10.1039/x0xx00000x

View Article Online
DOI: 10.1039/C8GC00801A

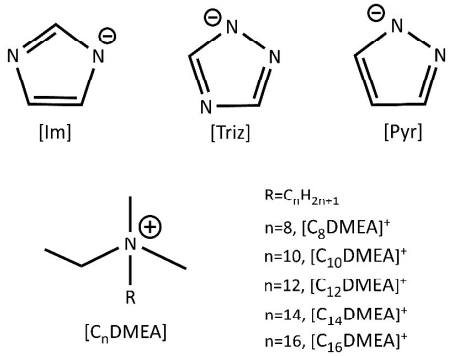

Scheme 1 Chemical structures of anions and cations of the studied ILs.

chloride ([C_{16}mim][Cl]) and 1-butyl-3-methylimidazolium triazolide ([C_4mim][tria123]). The former acts as a surfactant and the latter acts as a polar domain, but a cosurfactant (1-decanol) has to be added in the system. They investigated the phase transition of the microemulsion from a monophasic system to a turbid emulsion driven by CO_2. Dong et al.[17] proposed a temperature-induced reversible switching of amphiphilic self-assemblies between micelles and microemulsions by using a temperature-sensitive ionic liquid tetrabutylphosphonium trifluoroacetate ([P_{4444}][CF_3COO]) in Triton X-100-H_2O system. To our knowledge, reversible switching from ionic liquids based microemulsions to complete oil-water phase separation has not been reported so far.

Herein, we developed a class of CO_2-responsive microemulsions comprising IL, n-pentanol and water, where the ILs composed of N-alkyl-N,N-dimethylethylamine cation $[C_nDMEA]^+$ (n = 8, 10, 12, 14, 16) and azole-based anion, including imidazolium ($[Im]^-$), trizolium ($[Triz]^-$) and pyrazolium ($[Pyr]^-$) (Scheme 1), were employed as the surfactants in the formulation of our microemulsion systems. From phase diagram, electrical conductivity, dynamic light scattering, small-angle X-ray scattering, cryogenic transmission electron microscopy, optical microscope, and ^{13}C NMR spectrum investigations, it was found that these microemulsion systems underwent a reversible switching from an apparent water-in-n-pentanol monophase microemulsion to complete water-oil phase separation by alternatively bubbling and removal of CO_2 at atmospheric pressure. Such a CO_2-driven reversible phase separation was studied in detail and the results have been explained with the reversible formation of bicarbonate and carbamate from the reaction between CO_2 and anions of the ionic liquids in the systems. Based on this unique property of the microemulsions, the phase separation protocol was applied in Knoevenagel reaction for efficient coupling of chemical reaction, product separation, and recycling of the microemulsions.

Experimental section

Materials

1-Bromooctane ($C_8H_{17}Br$, 98 wt%), 1-bromodecane ($C_{10}H_{21}Br$, 98 wt%), 1-bromododecane ($C_{12}H_{25}Br$, 98 wt%), 1-bromotetradecane ($C_{14}H_{29}Br$, 98 wt%), 1-bromohexadecane ($C_{16}H_{33}Br$, 98 wt%), and anion exchange resin (Amersep 900 OH) were purchased from Alfa Aesar. N, N-dimethylethylamine (DMEA), imidazole (Im), trizole (Triz), and pyrazole (Pyr) were acquired from Aladdin. n-Pentanol was purchased from Sinopharm Chemical Reagent Co., Ltd. Double distilled water was used throughout the experiments. CO_2 (Praxair, SFC grade, 99.998 vol%) and N_2 (Praxair, 99.9993 vol%) were purchased from Beijing Praxair Application Gas Corp. All the chemicals were used as received unless otherwise stated.

Preparation of the ILs

[C_8DMEA][Br], [C_{10}DMEA][Br], [C_{12}DMEA][Br], [C_{14}DMEA][Br] and [C_{16}DMEA][Br] were synthesized and purified by the following procedures.[18,19] Briefly, N, N-dimethylethylamine and alkyl bromide ($C_8H_{17}Br$, $C_{10}H_{21}Br$, $C_{12}H_{25}Br$, $C_{14}H_{29}Br$ or $C_{16}H_{33}Br$) were mixed at a molar ratio of 1.1:1.0 (DMEA: alkyl bromide) in absolute ethanol, and the mixture was refluxed at 70 ^{o} C for 72 h under magnetic stirring. Then, ethanol was removed by rotary evaporation, and the products ([C_8DMEA][Br], [C_{10}DMEA][Br], [C_{12}DMEA][Br], [C_{14}DMEA][Br] and [C_{16}DMEA][Br]) were obtained by extraction with petroleum ether. The neat products were dried under vacuum for 12 h at 50 °C. Then, a solution of [C_8DMEA][OH], [C_{10}DMEA][OH], [C_{12}DMEA][OH], [C_{14}DMEA][OH] or [C_{16}DMEA][OH] in the mixed solvent of ethanol and water (1:1 volume ratio) was prepared by means of the anion-exchange method. Equimolar Im (Triz or Pyr) was added and the mixture was then stirred for 12 h at room temperature. After that, the solvent was distilled off at 45 ^{o}C by rotary evaporation.

The obtained products were dried for at least 24 h under reduced pressure. The chemical structures of these ILs were confirmed by ^1H NMR, ^{13}C NMR and IR spectroscopy (see supporting information). The residual bromide content in these azole-based ILs was determined by using the procedures reported previously.[20,21] It was found that the bromide content was less than 0.0090 mol kg^{-1} (Table 1). The purity (expressed in mole percent) of these ILs was determined by quantitative ^1H NMR measurements according to the method described by Xu et al.,[22] and the following results were obtained: [C_8DMEA][Im] (99.5%), [C_{10}DMEA][Im] (99.1%), [C_{12}DMEA][Im] (99.5%), [C_{14}DMEA][Im] (99.3%), [C_{16}DMEA][Im] (99.5%), [C_8DMEA][Pyr] (99.0%), [C_{10}DMEA][Pyr] (98.8%), [C_{12}DMEA][Pyr] (99.0%), [C_{14}DMEA][Pyr] (99.5%), [C_{16}DMEA][Pyr] (99.5%), [C_8DMEA][Triz] (99.5%), [C_{10}DMEA][Triz] (99.0%), [C_{12}DMEA][Triz] (98.7%), [C_{14}DMEA][Triz] (99.2%) and [C_{16}DMEA][Triz] (99.5%).

Measurements of NMR, IR spectrum, melting point and thermal decomposition temperature

^1H NMR and ^{13}C NMR spectra of these ILs were recorded on a Bruker spectrometer (400 MHz). FTIR spectrum was measured by using a PerkinElmer FTIR-400 spectrometer with universal ATR sampling accessory. Glass transition temperature (T_g) and melting point (T_m) were determined by a Netzsch 204F1 differential scanning calorimeter (DSC). Thermal decomposition temperature (T_d) was acquired with a Netzsch Sta 449 C thermal analyzer. Each experiment was carried out in triplicate, and average values were calculated.

View Article Online
DOI: 10.1039/C8GC00801A

Determination of Phase diagram

Phase diagram was constructed by adding a given IL into the mixtures of H_2O and alcohol at 25.0 ± 0.1 °C. For this purpose, a mixture with the desired mass ratio of the alcohol to water was prepared in a dry test tube. Then, an appropriate mass of the IL was added and the mass fraction of the IL at which turbidity-to-transparency occurred was calculated. Based on the critical values obtained at different mass ratios of alcohol to water, the phase boundary was established. The whole procedure was repeated three times, and an average value was acquired.

Electrical conductivity, optical microscopy and droplet size measurements of the microemulsions

Electrical conductivity measurements were carried out by using a DDSJ-308A conductivity meter (Shanghai Leici Precision Instrument Co., Ltd.) with an accuracy of ± 0.5%. The temperature was controlled by a precision DC-2006 bath circulator (Tianheng Precision Instrument Co., Ltd.) to be 25.0 ± 0.1 °C. The micrographs of microemulsion and emulsion droplets were recorded by using a DYP-990 microscope system (Shanghai Dianying Optical Instrument Co., Ltd.). For droplet size measurements by dynamic light scattering (DLS), all sample solutions were filtered through a 0.45 μm Millipore filter to remove any dust or contaminants and then kept at the measuring temperature for 12 h before determination. DLS measurements were performed by using a Malvern Zetasizer Nano-90 light scattering instrument (Malvern, United Kingdom) equipped with a solid-state He−Ne (4.0 mW) laser operating at λ = 633 nm. All the samples were measured at a scattering angle of 90° and 25.0 ± 0.1 °C.

Cryogenic transmission electron microscopy observation of the microemulsions

Cryogenic transmission electron microscopy (Cryo-TEM) samples were prepared by using a custom-built chamber. After the Cryo-TEM grid was fixed in the preparation chamber, a 5μL of sample solution was dropped on a carbon-coated holey film which was supported by a copper grid at room temperature. After the excess solution was blotted away to form a thin liquid film, the grid was quenched rapidly into liquid ethane cooled by liquid nitrogen (-175 °C), and then the specimen stored in liquid nitrogen was transferred into a JEOL JEM1400 cryomicroscope. The acceleration voltage was 200 kV, and the working temperature was kept approximately at -175 °C. The images were recorded digitally with a high speed charge coupled device (CCD) camera.

Small-angle X-ray scattering experiments

Small-angle X-ray scattering (SAXS) experiments were performed by using a sealed-tube Cu target (40kV, 40mA) instrument named SAXSess mc^2 (Anton Paar, Austria) which was equipped with a line-collimation Kratky block system and an image plate detector. Both parts were placed in vacuum chamber to avoid air scattering. The samples were held in a quartz capillary fixed in a stainless steel tank at 25 °C. Scattering data of sample and background were obtained in a 30 min exposure. Then the background scattering from empty sample holder was subtracted from sample curves after absorption correction. The scattering curves were output as the plot of scattering intensity vs the scattering vector, $q = (4\pi/\lambda)\sin\theta$ (2θ=scattering angle). Then pair distance distribution function (PDDF) was calculated by using the generalized indirect Fourier transform program package.

Results and discussion

Thermal properties of the ILs

Table 1 shows glass transition temperature (T_g), melting point (T_m) and thermal decomposition temperature (T_d) of these ILs. It was found that [C_8DMEA][Im], [C_8DMEA][Triz], [C_8DMEA][Pyr] and [C_{10}DMEA][Pyr] exhibited only glass transition temperature, and most of the other compounds had a melting point below 50 °C. This indicates that all these compounds are really ionic liquids. Additionally, thermal decomposition temperature of these ILs ranges from 140 to 188 °C, and the effect of alkyl chain length of the cations and type of anions is not significant. These results suggest that the ILs investigated here have good liquid temperature range and reasonable thermal stability.

Phase diagrams and microstructures of the microemulsion systems

To prove the formation of microemulsions in the homogeneous systems, the equilibrium phase diagrams of the n-pentanol/ILs/H_2O ternary systems were determined at 25.0 °C, and the results were shown in Fig. 1 for n-pentanol/[C_nDMEA][Im] (n = 8, 10, 12, 14, 16)/H_2O system. It is obvious that a wide monophasic region and a narrow biphasic region were obtained in all the phase diagrams. The monophasic region of the systems was only slightly changed as carbon atom number in the alkyl chain of the ILs increased from 8 to 16. Similar results were observed for n-pentanol/[C_nDMEA][Pyr] (n = 8, 10, 12, 14, 16)/H_2O (Fig. S1) and n-pentanol/[C_nDMEA][Triz] (n = 8, 10, 12, 14, 16)/H_2O systems (Fig. S2). Furthermore, the effect of anions of the ILs on the monophasic region of the n-pentanol/ILs/H_2O systems was

Table 1. Glass transition temperature (T_g)/melting point (T_m) and thermal decomposition temperature (T_d) of the ILs as well as Br^- content in the ILs.

IL	T_g (°C)	T_m (°C)	T_d (°C)	[Br^-]/mol kg^{-1}
[C_8DMEA][Im]	-65		153	0.0090
[C_{10}DMEA][Im]		30	174	0.0084
[C_{12}DMEA][Im]		46	175	0.0051
[C_{14}DMEA][Im]		54	188	0.0074
[C_{16}DMEA][Im]		79	183	0.0023
[C_8DMEA][Triz]	-72		140	0.0079
[C_{10}DMEA][Triz]		11	149	0.0074
[C_{12}DMEA][Triz]		34	143	0.0070
[C_{14}DMEA][Triz]		41	141	0.0074
[C_{16}DMEA][Triz]		49	159	0.0025
[C_8DMEA][Pyr]	-68		164	0.0075
[C_{10}DMEA][Pyr]	-60		177	0.0066
[C_{12}DMEA][Pyr]		28	187	0.0061
[C_{14}DMEA][Pyr]		31	168	0.0062
[C_{16}DMEA][Pyr]		44	165	0.0059

View Article Online
DOI: 10.1039/C8GC00801A

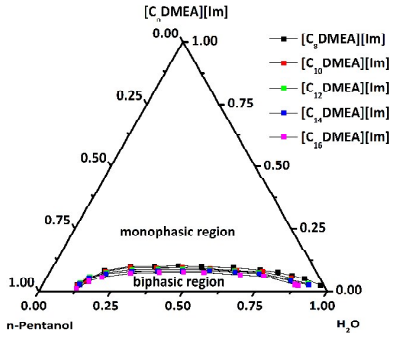

Fig. 1 Phase diagrams of the n-pentanol/[C_nDMEA][Im] (n = 8, 10, 12, 14, 16)/H_2O microemulsions (in mass fraction) at 25.0 °C.

also small (Fig. S3). These features are beneficial to the composition optimization of the microemulsion systems.

Next, electrical conductivity was measured to determine the microstructure of microemulsions at 25 °C. Taking n-pentanol/[C_{12}DMEA][Im]/H_2O system as an example, electrical conductivity was determined as a function of water mass fraction (W_0) at any given mass ratio of n-pentanol to the IL (I). Fig. 2a shows the conductivity at I = 1.0 and different water contents. It can be seen that with the increase of water content (W_0 < 0.32), conductivity initially increased gradually. Then, it quickly increased almost linearly with the increase of water content (W_0 < 0.68) and reached the maximum of conductivity. Finally, the conductivity decreased with increasing water content. The initial increase in conductivity may be owing to successive increase of conductivity of W/O microemulsion droplets with the addition of water.[23] The followed linear increase reveals that the system underwent a structural transition and became a bicontinuous (BC) microstructure.[23,24] The final decrease in conductivity can be interpreted from the consequence of the formation of O/W microemulsion resulted from the partial fusion of clustered inverse micro-droplets.[25] Similar conductivity change in the n-pentanol/[C_{12}DMEA][Im]/H_2O system with water content was also found at other I values, as shown in Fig. S4 (supporting information). Therefore, three different micro-regions, including H_2O-in-n-pentanol (W/O), bicontinuous region (BC),

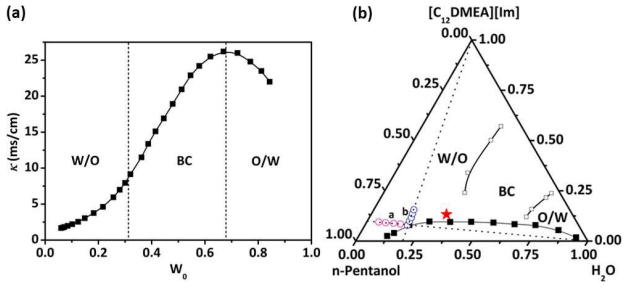

Fig. 2 Electrical conductivity of the n-pentanol/[C_{12}DMEA][Im]/H_2O microemulsion as a function of water content (W_0) at I = 1.0 and 25 °C (a); phase diagram of the n-pentanol/[C_{12}DMEA][Im]/H_2O microemulsion with different types of microstructure at 25.0 °C (b); circles (pink and blue) were results from DLS measurements; the red star represents the composition of the samples investigated in the next sections. The composition is expressed in mass fraction.

and n-pentanol-in-H_2O (O/W), were identified for the microemulsion (Fig. 2b). In addition, the microemulsion type was also identified by using drop test approach.[11,26] By placing a drop of each microemulsion on both water and oil phases, respectively, the microemulsion type could be determined through observing which phase the drop was easily dispersed into. It was found that the results were in good agreement with that determined from electrical conductivity measurements. Similar results were obtained for the n-pentanol/[C_nDMEA][Pyr] (n = 8, 10, 12, 14, 16)/H_2O (Figs. S5-S6) and n-pentanol/[C_nDMEA][Triz] (n = 8, 10, 12, 14, 16)/H_2O (Figs. S7-S8) systems.

The microstructure of H_2O-in-n-pentanol microemulsions was studied by using DLS and SAXS. Taking n-pentanol/[C_{12}DMEA][Im]/H_2O system as a representative example, samples with different compositions were chosen, as marked in Fig. 2b. The hydrodynamic diameter of the H_2O-in-n-pentanol microemulsion droplets were shown in Fig. 3a. It was shown that the size of the W/O microemulsion droplets increased (from 2.0 nm, 5.9 nm, 9.1 nm, 10.7 nm to 16.2 nm) with increasing molar ratio (R) of H_2O to [C_{12}DMEA][Im] from 9.28 to 57.01 at I = 9.0. The polydispersity index (PDI) values were found to be smaller than 0.23 (Table S1), which indicated a narrow size distribution and a homogeneous distribution of the aggregates in the microemulsions.[25] In addition, a linear correlation was observed between the size of the microemulsion droplets and the content of water (inset of Fig. 3a), which suggests the existence of spherical droplets in the IL-based microemulsions.[25] To confirm the effect of solution color on the size measurements of the microemulsion droplets, SAXS tests were performed for the n-pentanol/[C_{12}DMEA][Im]/H_2O microemulsion at different water contents. Representative SAXS and PDDF curves were shown in Fig. S9 and Fig. 3b, respectively. The SAXS curves further proved the

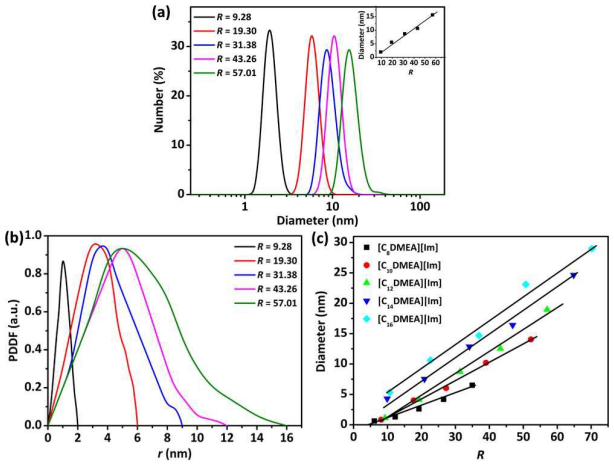

Fig. 3 Size distributions (a) and PDDF curves (b) of the n-pentanol/[C_{12}DMEA][Im]/H_2O microemulsion droplets at I = 9.0 (n-pentanol/[C_{12}DMEA][Im], 9:1, w/w) and different R values (molar ratio of H_2O to [C_{12}DMEA][Im]); Linear correlation of size of the [C_nDMEA][Im] (n= 8, 10, 12, 14, 16) microemulsion droplets with R values at 25 °C (c). Inset of (a) is the linear change of mean size with R values.

View Article Online
DOI: 10.1039/C8GC00801A

existence of droplets in the microemulsions. It was noted that each PDDF curve ascended and descended steeply before and after the maximum, and then decayed to zero at a certain *r* value, which indicates the droplet size of the microemulsions.[27] Thus, it could be seen that the droplet size derived from SAXS was about 2.0 nm, 6.0 nm, 8.8 nm, 12.0 nm and 16.0 nm at the given water contents. Obviously, the droplet size determined from SAXS was consistent with that from DLS measurements. Therefore, the effect of the solution color on the size measurements of the microemulsion droplets was negligible in this work.

The swelling behavior of the microemulsion with different contents of $[C_{12}DMEA][Im]$ was also investigated by DLS. For this purpose, n-pentanol/H_2O mass ratio was fixed at 4:1, but the molar ratio of H_2O to $[C_{12}DMEA][Im]$ (*R*) was changed to reflect the variation of the $[C_{12}DMEA][Im]$ content. It was shown that the droplet size of the n-pentanol/$[C_{12}DMEA][Im]$/H_2O microemulsion increased from 1.1 to 21.1 nm with the increase of *R* value from 17.96 to 40.40 (Fig. S10). This regular swelling behavior was in agreement with the volume of dispersed nanodomains being directly proportional to the amount of the added inner phase, which is common in many traditional microemulsions,[17] and suggests the formation of H_2O-in-n-pentanol microemulsions. Furthermore, microemulsions containing different alkyl chain lengths of ILs were also studied by using DLS. As shown in Fig. 3c, the size of the H_2O-in-n-pentanol microemulsions increased with increasing alkyl chain length of the ILs at a given *R* value. Therefore, the droplet size of the longer chain ILs-based microemulsions was much bigger than that of the shorter chain ILs-based microemulsions under the same conditions, which is consistent with the result reported in literature.[25] Similar trends were obtained for the n-pentanol/$[C_nDMEA][Pyr]$ (n = 8, 10, 12, 14, 16)/H_2O (Figs. S11-S13) and n-pentanol/$[C_nDMEA][Triz]$ (n = 8, 10, 12, 14, 16/H_2O (Figs. S14-S16) systems.

CO_2-driven reversible oil-water phase separation of the microemulsions

CO_2-responsive characteristics of the n-pentanol/ILs/H_2O microemulsions were investigated at 25.0 °C. Here, the n-pentanol/$[C_{12}DMEA][Im]$/H_2O microemulsion with the composition (marked by a red star in Fig. 2b) fixed at 54.2 wt% of n-pentanol, 13.3 wt% of $[C_{12}DMEA][Im]$, and 32.5 wt% of H_2O was studied as an example. It was shown that in the absence of CO_2, the microemulsion system was homogeneous (Fig. 4a). When CO_2 was bubbled through the system at approximately 2-3 bubbles per second under stirring at room temperature, it turned to be opaque emulsion in less than one minute (Fig. 4b). Further bubbling of CO_2 for about 30 min, the microemulsion was separated into two transparent phases (Fig. 4c). It can be seen from Fig. 4c that the lower aqueous phase was almost colorless while the upper organic phase was pale yellow, indicating transfer of the IL into the organic phase. Furthermore, the amount of the residual $[C_{12}DMEA][Im]$ in the aqueous solution after bubbling CO_2 was determined by spectrophotometric method.[11,28] It was obtained from Fig. S17

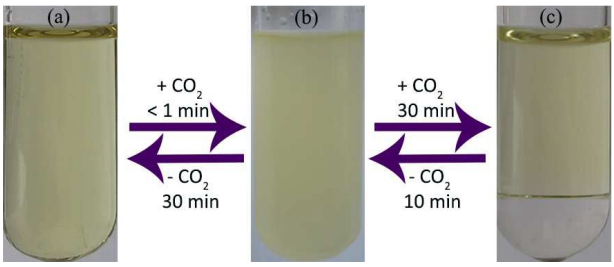

Fig. 4 Reversible switching of the n-pentanol/$[C_{12}DMEA][Im]$/H_2O microemulsion: monophasic W/O microemulsion before bubbling CO_2 (a), opaque emulsion after bubbling of CO_2 for less than 1 min (b), a clear phase separation of oil and water after bubbling CO_2 for 30 min (c).

that the concentration of the residul $[C_{12}DMEA][Im]$ in the aqueous solution is 74.5 mmol·L^{-1} (2.3 %). However, when CO_2 was removed by N_2 bubbling at 50 °C, the system returned to transparency again (Fig. 4a). Therefore, the ternary systems could be reversibly transformed upon alternatively bubbling and removal of CO_2. Similar reversible phase separation process was also observed for the other microemulsion systems investigated in this work.

Microstructures of the microemulsions after bubbling of CO_2 were investigated by DLS, Cryo-TEM and optical microscopy. For example, DLS result showed that the droplet size of the initial n-pentanol/$[C_{12}DMEA][Im]$/H_2O microemulsion was about 22.3 nm (Fig. 5). Upon bubbling of CO_2, it was increased to 3100 nm due to the disruption of the W/O microemulsion. When the W/O microemulsion was formed once again by bubbling of N_2 at 50 °C, the droplet size was decreased to 22.0 nm which was very close to its original value. Therefore, the n-pentanol/$[C_{12}DMEA][Im]$/H_2O microemulsion could be reversibly disrupted and re-formed with alternatively bubbling and removal of CO_2. Cryo-TEM images further showed that many well-dispersed spherical-like microstructures existed in the initial and recycled n-pentanol/$[C_{12}DMEA][Im]$/H_2O microemulsion (Figs. 6a and 6c). Furthermore, the size of the spherical-like structures from Cryo-TEM images was consistent with that from the DLS measurements (Figs. 6b and 6d).

In addition, optical microscope was applied to study the phase separation of microemulsions after bubbling of CO_2. As

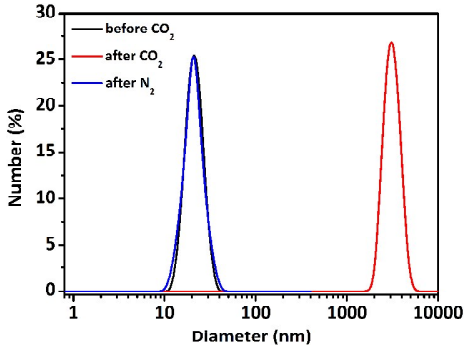

Fig. 5 Sizes of the n-pentanol/$[C_{12}DMEA][Im]$/H_2O microemulsion before bubbling CO_2 (black), after bubbling CO_2 (red), and after removal of CO_2 by bubbling N_2 at 50 °C (blue).

View Article Online
DOI: 10.1039/C8GC00801A

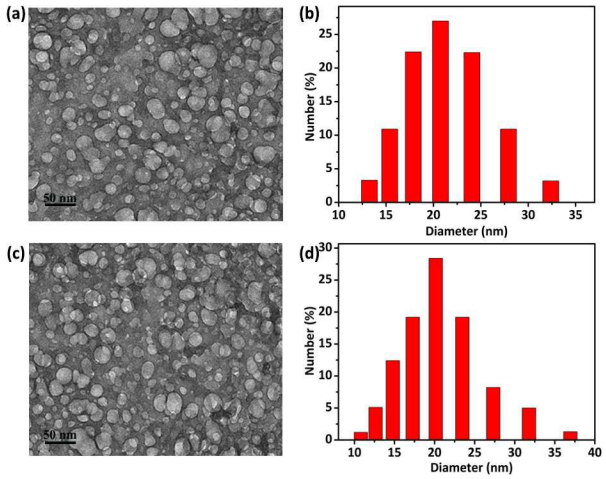

Fig. 6 Cryo-TEM images and droplet size distribution of the CO_2-switchable microemulsion: Cryo-TEM micrograph (a) and droplet size distribution (b) of the initial n-pentanol/$[C_{12}DMEA][Im]/H_2O$ microemulsion; Cryo-TEM micrograph (c) and droplet size distribution (d) of the n-pentanol/$[C_{12}DMEA][Im]/H_2O$ microemulsion after one cycle.

an example, the optical micrographs of n-pentanol/$[C_{12}DMEA][Im]/H_2O$ microemulsion were exhibited in Fig. 7. It is clear that no drops were found in initial n-pentanol/$[C_{12}DMEA][Im]/H_2O$ microemulsion because of their small size (Fig. 7a). Once CO_2 was bubbled into the system, numerous larger emulsion drops (~3 μm in diameter) appeared in the system (Fig. 7b). These emulsion drops were highly unstable due to their high interfacial energy. Thus by further bubbling of CO_2, these unstable drops gradually combined to form large drops that were more unstable. Finally, the emulsion was completely disrupted, and the drops were no longer visible (Fig. 7c).

Possible mechanism for CO_2-driven phase separation of the microemulsions

Considering the fact that the microemulsions studied in this work have N-containing heterocyclic anion such as $[Im]^-$, $[Pyr]^-$ and $[Triz]^-$ which can efficiently absorb CO_2,[15] phase separation of the microemulsions driven by CO_2 may be ascribed to the reaction of these anions with CO_2. To verify this speculation, ^{13}C NMR spectroscopy was used to probe the interactions between CO_2 and anions of the ILs in the n-pentanol/ILs/H_2O microemulsion systems before bubbling of CO_2 and after

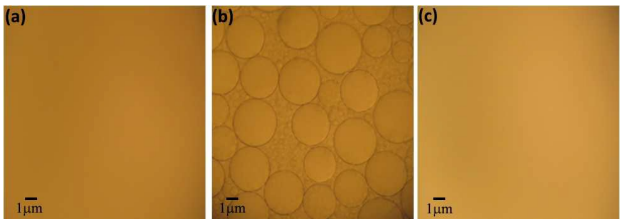

Fig. 7 The optical micrographs of the initial n-pentanol/$[C_{12}DMEA][Im]/H_2O$ microemulsion (a), the emulsion after CO_2 exposure for 10 min at room temperature (b), and the upper oil phase after CO_2 bubbling for 30 min at room temperature (c).

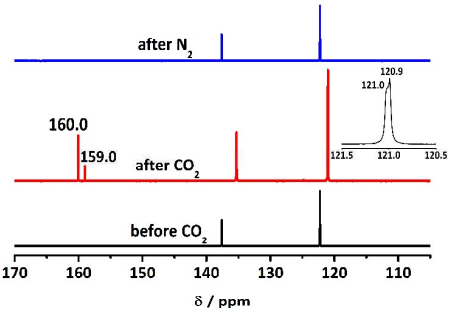

Fig. 8 ^{13}C NMR spectra of $[C_{12}DMEA][Im]$ in the n-pentanol/$[C_{12}DMEA][Im]/H_2O$ microemulsion before bubbling of CO_2 and after bubbling of N_2 as well as in the aqueous solution after phase separation.

bubbling of N_2 as well as in the aqueous solution after phase separation (the lower phase in Fig. 4c). Since the concentrations of the ILs in aqueous solutions after phase separation were small, these solutions were concentrated before measurements. As an example, ^{13}C NMR spectrum of $[C_{12}DMEA][Im]$ in the systems mentioned above was determined at 25 °C, and the results were shown in Fig. 8. It is clear that after phase separation, two new signals appeared at 159.0 and 160.0 ppm in the ^{13}C NMR spectrum of $[C_{12}DMEA][Im]$ in aqueous solution. The signal at 160.0 ppm could be ascribed to the carbonyl carbon of bicarbonate generated from the reaction of $[Im]^-$ anion with CO_2 in the presence of water.[18,29] Additionally, the signal at 159.0 ppm was identified to be the carbonyl group of the carbamate $[ImCO_2]^-$ formed from the reaction between CO_2 and $[Im]^-$ anion, and the chemical shift and signal intensity were very close to those reported previously.[15,30] The strong signal at 120.9 ppm was mainly assigned to the Im molecule, and the small shoulder at 121.0 ppm indicated the formation of the unsymmetrical monocarbamate.[18] The former indicates that Im molecules were formed after bubbling of CO_2. On the other hand, the spectrum of the IL after removal of CO_2 by bubbling of N_2 was found to be the same with that before bubbling of CO_2 (that is, in the initial microemulsion). Similar results were obtained for the interactions of CO_2 with anions of $[C_nDMEA][Pyr]$ (n = 8, 10, 12, 14, 16) (Fig. S18) and $[C_nDMEA][Triz]$ (n = 8, 10, 12, 14, 16) (Fig. S19). Therefore, it can be deduced that the mechanism behind the reversible switching of the microemulsions may involve the reversible formation of ammonium salts (bicarbonate and carbamate) from the reaction between the anions and CO_2. This results in the increase of ionic strength (or vice versa) in the mixtures, and the salting-out effect makes the microemulsions to be disrupted.[31] The reversible change in ionic strength gives rise to the reversible switching from a single phase microemulsion to a clear oil-water phase separation.

In order to confirm that the phase separation of the microemulsions was caused by the increase of ionic strength in the systems, NaCl, $NaHCO_3$, and Na_2CO_3 were chosen to examine the effect of ionic strength on the stability of microemulsions. As an example, Fig. S20 shows the effect of $NaHCO_3$ content on the droplet size of n-pentanol/

View Article Online
DOI: 10.1039/C8GC00801A

$[C_{12}DMEA][Im]/H_2O$ microemulsion determined by DLS. It was shown that when $NaHCO_3$ content in the system was increased from 0 to 83.32 mmol·L^{-1}, the droplet size changed remarkably from 22.0 nm (without salt) to 2305 nm, and obvious phase separation was observed at $NaHCO_3$ concentration of 35.71 mmol·L^{-1}. Based on the above results, it can be concluded that the oil-water phase separation of microemulsions was ascribed to the increase of ionic strength in the mixture.

Application of the CO_2-responsive microemulsions as microreactors for organic reaction

Knoevenagel condensation reaction is a general and important reaction for the formation of carbon-carbon bond, and has been widely applied to synthesize a number of important fine chemicals and heterocyclic compounds.[32-34] As a proof of concept, our microemulsions were used as microreactors for Knoevenagel reaction to demonstrate the coupling of chemical reaction, product separation and recycling of the microemulsions. As shown in Fig. 9, the reaction for the preparation of 2-benzylidenemalononitrile proceeded well in the n-pentanol/$[C_{12}DMEA][Im]/H_2O$ microemulsions at 25 °C. Upon bubbling of CO_2 for less than 10 min, the microemulsion was disrupted, and the product was precipitated from the reaction system and suspended in the water phase. Then, the product was filtered out from the water phase. On the other hand, when CO_2 was removed by N_2 bubbling, the microemulsion was regenerated, and once new reactants were added in the system, the same reaction happened again.

Then, the product 2-benzylidenemalononitrile was identified by ^{1}H NMR spectroscopy (see Fig. S21), and the yield was up to 97.2%. After three recycles, its yield still reached to 94.5% (Fig. S22). Besides, it was found that the yield for the same reaction in different microemulsions decreased in the order: $[C_{12}DMEA][Im]$ based microemulsion (97.2%) > $[C_{12}DMEA][Triz]$ based microemulsion (81.1%) > $[C_{12}DMEA][Pyr]$ based microemulsion (75.3%), indicating that the microemulsions with stronger basicity showed higher catalytic activity for Knoevenagel reactions.[18,35] To extend the substrate scope, several benzaldehyde derivatives were chosen to react with malononitrile under the same conditions and excellent yields were obtained (Table S2 and Figs. S23-S27). Comparing with other catalytic systems,[36,37] the microemulsions reported here exhibited superior catalytic activity for the Knoevenagel reaction. The resulting products could be easily separated from the reaction mixture by filtration, and the microemulsions could be readily recovered and recycled.

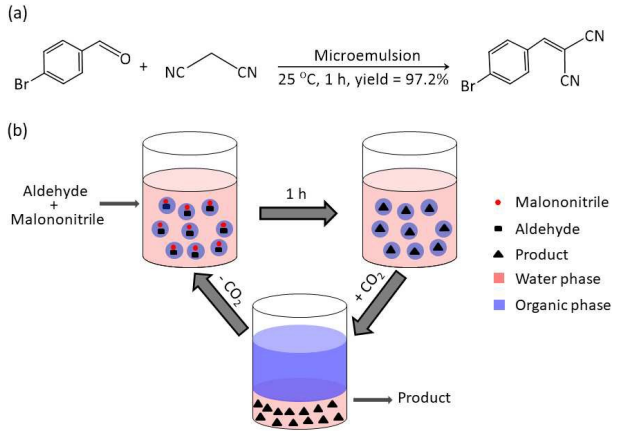

Fig. 9 Reaction between benzaldehyde and malononitrile in the n-pentanol/$[C_{12}DMEA][Im]/H_2O$ microemulsions (a), and the coupling of chemical reaction, product separation and recycling of the microemulsions (b).

Conclusions

We have demonstrated a class of simple stimuli-responsive microemulsions composed of CO_2-responsive ILs, n-pentanol and water. It was found that these systems underwent a reversible switching from a monophasic W/O microemulsion to complete oil-water phase separation by alternatively bubbling and removal of CO_2 at atmospheric pressure. The reversible phase separation of the microemulsion was ascribed to the reversible change (increase and decrease) of ionic strength in the systems due to the reversible formation of bicarbonate and carbamate from the reaction between CO_2 and anions of the ILs in the presence of water. Therefore, these microemulsions can be formed or disrupted on demand by using CO_2/ N_2 as a cheap and green trigger. By utilizing the CO_2-responsive property of these microemulsions, a highly efficient Knoevenagel reaction in microemulsion and simple product separation in aqueous phase was achieved. Additionally, the microemulsions could be reused for at least three runs without any significant impact on the yield of the products. These findings are significant for the development of new strategies for sustainable chemical processes.

Conflicts of interest

There are no conflicts to declare.

Acknowledgements

This work is supported by the National Natural Science Foundation of China (No. 21603063, U1704251 and 21733011), the National Key Research and Development Program of China (2017YFA0403101), and the 111 Project (No. D17007).

Notes and references

1 J. Klier, C. J. Tucker, T. H. Kalantar and D. P. Green, *Adv. Mater.*, 2000, **12**, 1751-1757.
2 M. Moniruzzaman, N. Kamiya and M. Goto, *J. Colloid Interface Sci.*, 2010, **352**, 136-142.
3 M. Schwarze, T. Pogrzeba, I. Volovych and R. Schomäcker, *Catal. Sci. Technol.*, 2015, **5**, 24-33.
4 J. G. E. M. Fraaije, K. Tandon, S. Jain, J.-W. Handgraaf and M. Buijse, *Langmuir*, 2013, **29**, 2136-2151.
5 A. V. Singh, Z. Hosseinidoust, B.-W. Park, O. Yasa and M. Sitti, *ACS Nano*, 2017, **11**, 9759-9769.

View Article Online
DOI: 10.1039/C8GC00801A

6 A. K. Ganguli, A. Ganguly and S. Vaidya, *Chem. Soc. Rev.*, 2010, **39**, 474-485.
7 T. Aouak, S. Moulay and A. Hadj-Ziane, *J. Membr. Sci.*, 2000, **173**, 149-157.
8 B. A. Kelser, D. Varie, R. E. Barden and S. L. Holt, *J. Phys. Chem.*, 1979, **83**, 1276-1280.
9 H. H. Ingelsten, J.-C. Béziat, K. Bergkvist, A. Palmqvist, M. Skoglundh, Q. Hu, L. K. L. Falk and K. Holmberg, *Langmuir*, 2002, **18**, 1811-1818.
10 R. F. Tabor, R. J. Oakley, J. Eastoe, C. F. J. Faul, I. Grillo and R. K. Heenan, *Soft Matter*, 2009, **5**, 78-80.
11 Y. Zhang, Y. Zhang, C. Wang, X. Liu, Y. Fang and Y. Feng, *Green Chem.*, 2016, **18**, 392-396.
12 D. Liu, Y. Suo, J. Tan and H. Lu, *Soft Matter*, 2017, **13**, 3783-3788.
13 N. V. Plechkova and K. R. Seddon, *Chem. Soc. Rev.*, 2008, **37**, 123-150.
14 V. I. Pârvulescu and C. Hardacre, *Chem. Rev.*, 2007, **107**, 2615-2665 .
15 G. Cui, J. Wang and S. Zhang, *Chem. Soc. Rev.*, 2016, **45**, 4307-4339.
16 P. Brown, M. J. Wasbrough, B. E. Gurkan and T. A. Hatton, *Langmuir*, 2014, **30**, 4267-4272.
17 B. Dong, X. Xing, R. Wang, B. Wang, X. Zhou, C. Wang, L. Yu, Z. Wu and Y. Gao, *Chem. Commun.,* 2015, **51**, 11119-11122.
18 D. Xiong, G. Cui, J. Wang, H. Wang, Z. Li, K. Yao and S. Zhang, *Angew. Chem. Int. Ed.*, 2015, **54**, 7265-7269.
19 Y. Shi, D. Xiong, H. Wang, Y. Zhao and J. Wang, *Langmuir*, 2016, **32**, 6895-6901.
20 K. R. Seddon, A. Stark and M. J. Torres, *Pure Appl. Chem.*, 2000, **72**, 2275−2287.
21 J. Yang, H. Wang, J. Wang, Y. Zhang and Z. Guo, *Chem. Commun.*, 2014, **50**, 14979-14982
22 A. Xu, Y. Zhang, Z. Li and J. Wang, *J. Mol. Liq.*, 2016, **214**, 192-195.
23 M. L. Klossek, D. Touraud and W. Kunz, *Green Chem.*, 2012, **14**, 2017-2023.
24 M. Kaur, G. Singh, S. Kumar, Navnidhi and T. S. Kang, *J. Colloid Interface Sci.*, 2018, **511**, 344-354.
25 Y. Pei, Y. Huang, L. Li and J. Wang, *J. Chem. Thermodynamics*, 2014, **74**, 231-237.
26 W. Kong, S. Guo, S. Wu, X. Liu and Y. Zhang, *Langmuir*, 2016, **32**, 9846-9853.
27 Y. Pei, J. Ru, K. Yao, L. Hao, Z. Li, H. Wang, X. Zhu and J. Wang, *Chem. Commun*., 2018, DOI: 10.1039/c8cc02901f.
28 S. Li and S. Zhao, *Anal. Chim. Acta*, 2004, **501**, 99-102.
29 X. Pei, D. Xiong, J. Fan, Z. Li, H. Wang and J. Wang, *Carbon*, 2017, **117**, 147-153.
30 D. J. Heldebrant, P. K. Koech, M. T. C. Ang, C. Liang, J. E. Rainbolt, C. R. Yonker and P. G. Jessop, *Green Chem.*, 2010, **12**, 713-721.
31 S. M. Mercer and P. G. Jessop, *ChemSusChem*, 2010, **3**, 467-470.
32 A. Lee, A. Michrowska, S. Sulzer-Mosse and B. List, *Angew. Chem. Int. Ed.*, 2011, **50**, 1707-1710.
33 X. Garrabou, B. I. M. Wicky and D. Hilvert, *J. Am. Chem. Soc.*, 2016, **138**, 6972-6974.
34 S. K. Dey, N. S. Amadeu and C. Janiak, *Chem. Commun.*, 2016, **52**, 7834-7837.
35 G. Wu, S. Jiang, L. Li and N. Guan, *Appl. Catal. A: Gen.*, 2011, **391**, 225-233.
36 G. Tuci, L. Luconi, A. Rossin, E. Berretti, H. Ba, M. Innocenti, D. Yakhvarov, S. Caporali, C. Pham-Huu and G. Giambastiani, *ACS Appl. Mater. Interfaces*, 2016, **8**, 30099-30106.
37 T. Wu, X. Wang, H. Qiu, J. Gao, W. Wang and Y. Liu, *J. Mater. Chem.*, 2012, **22**, 4772-4779.